Structure of Bacteriophage P22 Portal Protein in Relation to Assembly: Investigation by Raman Spectroscopy†

Arantxa Rodríguez-Casado,‡ Sean D. Moore,§,|| Peter E. Prevelige, Jr.,§ and George J. Thomas, Jr.*,‡

Division of Cell Biology and Biophysics, School of Biological Sciences, University of Missouri−Kansas City, Kansas City, Missouri 64110-2499, and Department of Microbiology, University of Alabama at Birmingham, Birmingham, Alabama 35205

Received May 22, 2001; Revised Manuscript Received August 24, 2001

ABSTRACT: *Salmonella* phage P22, which serves as an assembly paradigm for icosahedral double-stranded DNA viruses, packages its viral genome through a capsid channel (portal) comprising 12 copies of a 725-residue subunit. Secondary and tertiary structures of the portal subunit in monomeric and dodecameric states have been investigated by Raman spectroscopy using a His_6-tagged recombinant protein that self-assembles in vitro [Moore, S. D., and Prevelige, P. E., Jr. (2001) *J. Biol. Chem. 276*, 6779−6788]. The portal protein exhibits Raman secondary structure markers typical of a highly α-helical subunit fold that is little perturbed by assembly. On the other hand, Raman markers of subunit side chains change dramatically with assembly, an indication of extensive changes in side chain environments. The cysteinyl Raman signature of the portal consists of a complex pattern of sulfhydryl stretching bands, revealing diverse hydrogen-bonding states for the four S−H groups per subunit (Cys 153, Cys 173, Cys 283, and Cys 516). Upon assembly, the population of strongly hydrogen-bonded S−H groups decreases, while the population of weakly hydrogen-bonded S−H groups increases, implying that specific intrasubunit S−H···X hydrogen bonds must be weakened to effect dodecamer assembly and that the molecular mechanism involves reorganization of subunit domains without appreciable changes in domain conformations. Comparison with other viral protein assemblies suggests an assembly process not requiring metastable intermediates. The recently published X-ray structure of the φ29 portal [Simpson, A. A., et al. (2000) *Nature 408*, 745−750] shows that residues 125−225 lining the channel surface form α-helical modules spaced by short β-strands and turns; a surprisingly close secondary structure homology is predicted for residues 240−350 of the P22 portal, despite no apparent sequence homology. This motif is proposed as an evolutionarily conserved domain involved in DNA translocation.

The *Salmonella* bacteriophage P22 has been investigated extensively as a model for icosahedral capsid assembly (*1*, *2*) and a prototype for morphogenesis of mammalian viruses (*3*−*5*). A key step in P22 assembly is packaging of the viral genome in an ATP-dependent reaction (*6*), involving translocation of double-stranded DNA through a specialized channel (portal) located at a unique vertex of the capsid precursor shell (procapsid). DNA also exits through the portal during host infection. Construction of a procapsid that is able to package DNA and undergo expansion to the mature capsid requires 420 copies of the coat subunit (gp5, 47 kDa), ∼300 copies of the scaffolding subunit (gp8, 34 kDa), and 12 copies of the portal subunit (gp1, 84 kDa) (*7*). The concatemeric phage DNA is packaged in a headful manner through the actions of the terminase proteins (gp2 and gp3). DNA packaging results in expulsion of scaffolding subunits through orifices in the procapsid lattice with concurrent expansion to the mature capsid. The portal itself is closed by the binding of minor proteins gp4, gp10, and gp26. Attachment of up to six trimeric tailspikes (gp9) results in the infectious phage particle (Figure 1). Coassembly of the topologically correct portal and shell from their respective subunits, retention of the portal ring during shell expansion, participation of the portal in ATPase-catalyzed DNA translocation events, and subsequent tailspike attachment all suggest a highly versatile portal protein that may undergo extensive switching between different conformational states in a specific path-dependent manner.

Portal assemblies of several DNA bacteriophages have been probed by structural and molecular biological methods (reviewed in refs *6* and *8*). Recently, a 3.2 Å resolution crystal structure (*9*) and DNA packaging model, consistent with electron cryomicroscopy image reconstructions (*10*, *11*), have been reported for the dodecameric portal of phage φ29. The phage SPP1 portal, also investigated by electron microscopy (*12*, *13*), exhibits 13-fold rather than 12-fold symmetry of φ29 and P22 portals. No high-resolution structure exists for the P22 portal; however, the subunit secondary structure and oligomerization pathway have been studied using biochemical and biophysical methods (*14*). Conversely, no structural information is available for the

† Supported by NIH Grants GM50776 (G.J.T.) and GM47980 (P.E.P.). Paper LXXVI in the series Structural Studies of Viruses by Raman Spectroscopy.

* To whom correspondence should be addressed. E-mail: thomasgj@umkc.edu. Telephone: (816) 235-5247. Fax: (816) 235-1503.

‡ University of Missouri−Kansas City.

§ University of Alabama at Birmingham.

|| Current address: Department of Biology, Building 68-571, Massachusetts Institute of Technology, Cambridge, MA 02139.

10.1021/bi0110488 CCC: $20.00
Published on Web 10/20/2001

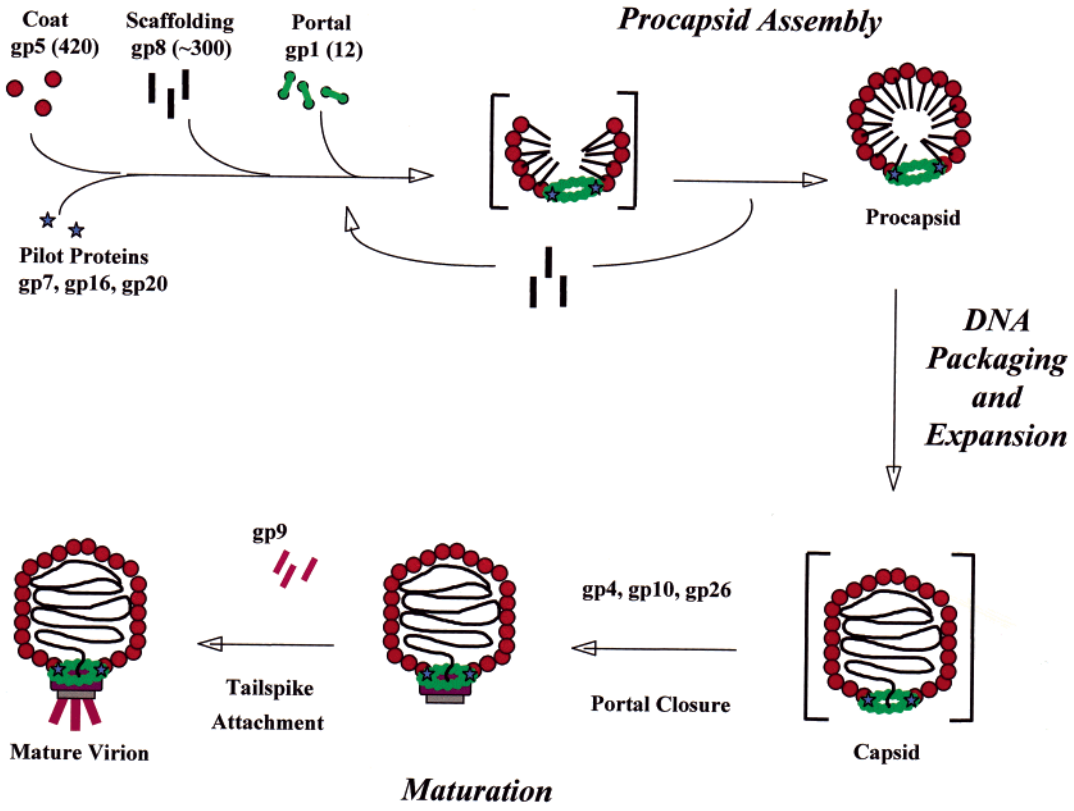

FIGURE 1: Assembly pathway of bacteriophage P22 (*46*, *47*) proceeding clockwise from the top left. Coassembly of 420 copies of the coat subunit (gp5), 12 copies of the portal subunit (gp1), and ~300 copies of the scaffolding subunit (gp8), together with a few copies of minor proteins (gp7, gp16, and gp20), leads to formation of the procapsid, which subsequently matures to the icosahedral capsid at the time of DNA packaging and scaffold ejection. The ATP-driven DNA packaging event is accomplished with the aid of a virally encoded phosphatase and additional minor proteins (terminase subunits gp2 and gp3) not shown. Portal closure by minor proteins (gp4, gp10, and gp26) and attachment of six trimeric tailspikes (gp9) lead to the mature virion.

monomeric states of portal subunits of φ29 and SPP1, even though they are considerably smaller (36 and 57 kDa, respectively) than that of P22 (84 kDa).

In all cases examined so far, the portal ring differs in symmetry from the 5-fold capsid vertex to which it is attached. While details of the portal−capsid interface are not understood, it has been suggested that a symmetry mismatch could facilitate portal rotation as the packaging mechanism (*15*). This concept has been incorporated into the packaging model proposed for the φ29 portal (*9*). Further insights into the subunit structure and molecular mechanism of assembly of the P22 portal are expected from analysis by Raman spectroscopy. Advantages of Raman spectroscopy for this purpose have been demonstrated recently in studies of the P22 procapsid shell, mature capsid shell, and trimeric tailspike (*16*−*19*), and in analogous studies of the DNA phage PRD1 and RNA phage φ6 (*20*−*22*).

Here, we report and interpret Raman spectra of the P22 portal subunit in monomeric and dodecameric states. The Raman spectra complement circular dichroism (CD) and fluorescence data (*14*), which collectively indicate the dependence of portal subunit structure on assembly state. Assembly-dependent Raman markers of key residues of the portal subunit are identified. Importantly, the findings presented here identify potentially productive targets for site-directed mutagenesis of the portal subunit and suggest an evolutionarily conserved domain that may line the portal channel and mediate viral genome translocation.

MATERIALS AND METHODS

Protocols for expression of the portal subunit (P22 gene *1* with a Leu-Glu linker and a His_6 tag ligated into a pET-21b plasmid) in *Escherichia coli* BL21(DE3) and purification by Ni affinity chromatography have been given elsewhere (*14*). The monomer and oligomer were separated using a combination of anion-exchange and size-exclusion chromatography. On the basis of a calculated molar extinction coefficient of 99 740 M^{-1} cm^{-1} at 280 nm (ϵ_{280}) for the denatured subunit (*23*), we obtained a yield of ~12−15 mg of purified monomer from 100 mL of culture.

Solutions of the monomer and oligomer (ring) were concentrated for Raman spectroscopy using a Centricon-10 instrument (Amicon, Danvers, MA) with a 30 kDa cutoff. Samples were assessed by size-exclusion chromatography before and after data collections to confirm protein integrity. Typically, an aliquot of protein solution (~5 μL) was transferred to a glass capillary (Kimax 34502), which was sealed and thermostated at 4 °C for data collection. The monomer and dodecamer were investigated at several protein concentrations (20−100 μg/μL) in 25 mM NaCl, 1 mM EDTA, and 20 mM Tris-HCl (pH 7.4) and exhibited concentration-independent Raman amide markers. Data shown below were obtained for solution concentrations in the range of 80−100 μg/μL. Raman spectra were excited with ~30 mW of 532 nm radiation (Verdi Nd:Y:VO_4 laser, Coherent Inc., Santa Clara, CA) and collected on a single spectrograph (model 500M, SPEX Inc., Edison, NJ) equipped

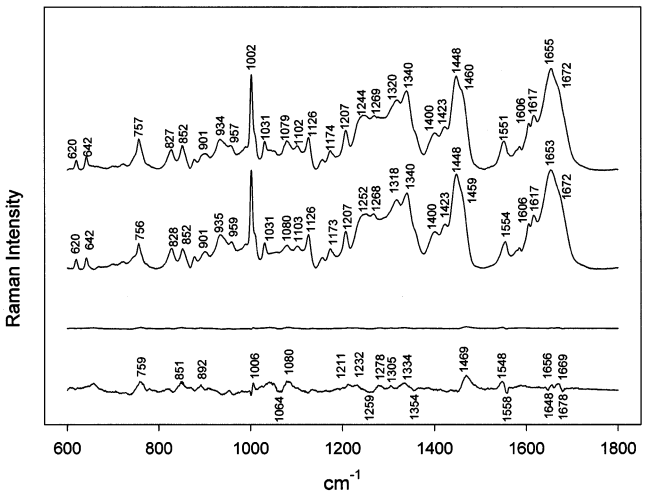

FIGURE 2: Raman spectra (600−1800 cm^{-1}, 532 nm excitation) of the P22 portal protein monomer (middle trace) and dodecamer (top trace) and the digital difference spectrum (second trace from the bottom) obtained by subtracting the spectrum of the monomer from that of the ring. Also shown (bottom trace) is an approximate 3-fold amplification of the difference spectrum. Proteins were dissolved to a final concentration of 40 mg/mL in 20 mM Tris (pH 7.5), 100 mM NaCl, and 2 mM EDTA. Spectra were corrected for contributions of the buffer solution and the gently sloping background typical of protein Raman spectra. Identical spectra were obtained for protein concentrations in the range of 25−100 mg/mL.

with a holographic notch filter, holographic grating, and a liquid nitrogen-cooled, charge-coupled-device detector. Further details of the instrumentation and sample handling procedures have been described previously (*25*).

RESULTS AND INTERPRETATION

Overview of the Raman Spectra

Recent developments in Raman instrumentation, including improved performance of spectrometers and detectors, now enable applications to relatively dilute solutions of proteins and exploitation of digital difference methods for detecting changes in local environments of side chains and conformations of the protein main chain (*26*−*28*). Substantial progress has also been made recently in identifying novel Raman markers of protein secondary, tertiary, and quaternary interactions (*16*, *29*−*31*). These developments are exploited in this study of the recombinantly produced P22 portal protein subunit. The focus is on interpretation of key Raman markers of the portal subunit side chains (Tyr, Trp, and Cys) and main chain (amide I and amide III bands) for monomeric and dodecameric (ring) states of the protein and on identification of the assembly-related structural changes. The results are compared with those obtained in Raman applications to other structural proteins of the P22 virion (*17*−*19*).

Raman Signature of the Monomeric Portal Subunit

The Raman spectrum of the monomeric portal subunit is shown in the middle trace of Figure 2. The major amide I band at 1653 ± 1 cm^{-1} (assigned to α-helix and irregular conformations) and the shoulder at 1672 ± 2 cm^{-1} (*β*-strand) indicate an α/*β*-fold with the α-helix predominating. To estimate the secondary structure distribution in the monomeric portal subunit, we employed a reference intensity

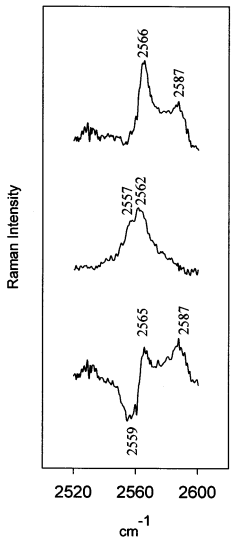

FIGURE 3: Raman spectra (2520−2600 cm^{-1}, 532 nm excitation) of the P22 portal protein monomer (middle trace) and dodecamer (top trace) and the digital difference spectrum (bottom trace) obtained by subtracting the spectrum of the monomer from that of the ring. Other conditions are as given in the legend of Figure 2.

profile method (*32*) for the amide I band contour of Figure 2. This method gives the following secondary structure distribution for the monomer: 56.6 ± 3.0% α-helix, 26.3 ± 0.8% *β*-strand, and 17.0 ± 1.3% other structure (i.e., irregular conformations, loops, turns, etc.). Uncertainties reflect the estimated precision of the method.

In the conformationally sensitive amide III region of the Raman spectrum (1225−1300 cm^{-1}), the monomer exhibits intense bands at 1252 and 1268 cm^{-1}. The former is very broad and contains contributions from both *β*-strand and irregular conformations, whereas the latter is relatively sharp and can be assigned to α-helical secondary structure. Thus, both the amide III and amide I profiles of the portal monomer are consistent with an α/*β*-fold in which the α-helix component is dominant.

The high α-helicity of the portal monomer is further supported by the prominent Raman band at 935 cm^{-1}, which originates from a coupled main chain and side chain mode common to α-helical proteins (*33*, *34*). The occurrence of a strong band at 1340 cm^{-1} is also indicative of a highly α-helical protein (*30*).

The Raman spectrum of the portal monomer is rich in bands originating from various side chains. Structurally informative markers of tyrosine (at 642, 828, 852, 1207, and 1617 cm^{-1}) and tryptophan (at 756, 878, 1554, 1579, and 1585 cm^{-1}) residues occur prominently in the spectral range shown in Figure 2. Of particular interest are Raman markers diagnostic of the sulfhydryl (S−H) groups of the four cysteine residues per subunit (Cys 153, Cys 173, Cys 283, and Cys 516), which occur uniquely in the 2520−2600 cm^{-1} interval of the spectrum, as shown in Figure 3 (middle trace). A comprehensive summary of Raman band assignments for the portal subunit is given in Table 1.

Raman Signature of the Dodecameric Portal Ring and Structural Significance of Spectral Changes with Assembly

The Raman spectrum of the dodecameric portal ring (Figure 2, top trace) is compared with that of the monomer

Table 1: Raman Bands and Assignments for the Portal Protein Subunit of Bacteriophage P22

Raman band (cm^{-1})[a]	relative intensity[b]	assignment[c]
620	5.8	Phe (ring str)
642	6.0	Tyr (ring str)
722	5.6	
756	6.8	Trp (ring str)
828	6.3	Tyr (ring str)
852	6.4	Tyr (ring str)
878	5.8	Trp (ring str)
901	6.0	
935	6.7	al (C−C str, CH_3 def)
959	6.4	al (C−C str, CH_3 def)
1002	9.7	Phe (ring str)
1031	6.6	Phe (ring str)
1080	6.6	nar (C−N, C−C str), Arg (C−C═N str)
1103	6.4	Ala (C−C str)
1126	6.8	nar (C−C str), Trp (ring str)
1155	5.8	al (CH_3 def)
1173	6.2	al (CH_3 def)
1207	7.1	Tyr (ring str)
1252	7.8	(amide III)
1268	7.8	(amide III)
1318	8.5	nar (CH_2 def)
1340	9.0	nar (CH_2 def)
1400	7.0	Asp, Glu (CO_2^- str)
1423	7.3	al (CH_3 def), Gly (CH_2 def)
1448	9.7	nar (CH_2 def)
1554	6.6	Trp (ring str)
1579	6.2	Trp (ring str)
1585	6.4	Trp (ring str)
1606	7.5	Phe (ring str)
1617	7.8	Tyr (ring str)
1653	10.0	α-helix (amide I)
1672	9.0	*β*-strand (amide I)
2557		Cys (S−H str)
2562		Cys (S−H str)

[a] Wavenumber units. [b] Arbitrary 0−10 scale, based upon 10.0 for the strongest band (1655 cm^{-1}) in the region of 600−1800 cm^{-1}. The intensities of the sulfhydryl bands at 2557 and 2562 cm^{-1} are approximately 10^{-2} of that of the 1655 cm^{-1} band. [c] Assignments are based upon studies of related proteins and model compounds. See, for example, refs *19*, *36*, and *45* and citations therein. Abbreviations: str, stretch; al, unspecified aliphatic side chain(s); def, deformation; nar, unspecified nonaromatic side chain(s).

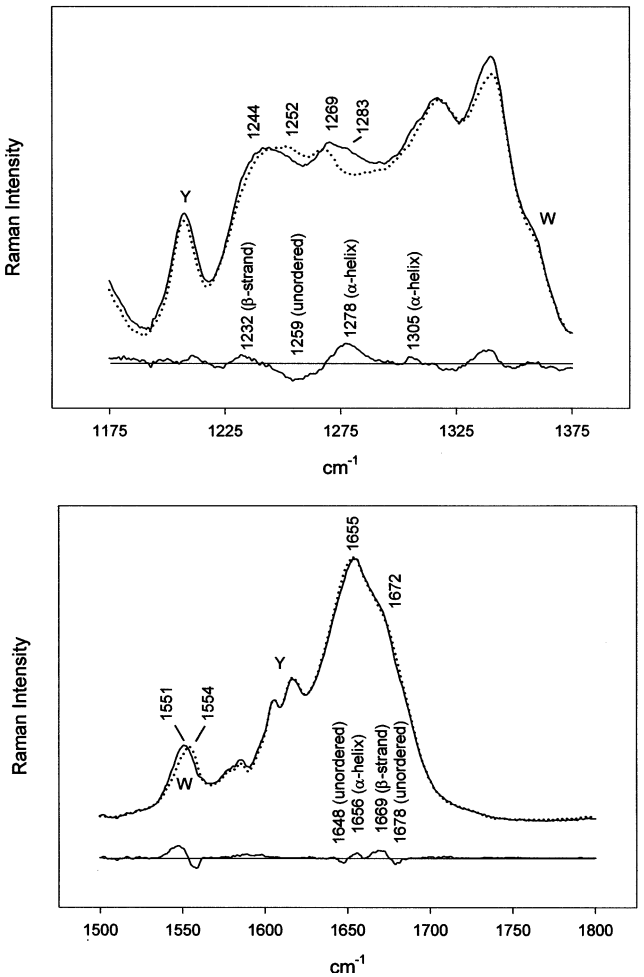

FIGURE 4: (Top panel) Raman spectra in the region of 1175−1375 cm^{-1} of the P22 portal protein monomer (•••) and dodecamer (—) and their corresponding digital difference spectrum (bottom trace). Prominent Raman amide III markers and their difference peaks and troughs are labeled in the bottom trace. (Bottom panel) Raman spectra in the region of 1500−1800 cm^{-1} of the P22 portal protein monomer (•••) and dodecamer (—) and their corresponding digital difference spectrum (bottom trace). Prominent Raman amide I markers and their difference peaks and troughs are labeled in the bottom trace.

(Figure 2, second trace from the top) by digital difference (Figure 2, bottom two traces). The assembly-related perturbations observed for numerous side chain Raman markers, as well as for Raman amide I and amide III main chain markers, are significant and reproducible. Most striking are the changes observed in the 2520−2600 cm^{-1} region (Figure 3), which indicate major alterations in cysteine S−H hydrogen bonding. The data show that environments of both aromatic and nonaromatic side chains are greatly perturbed by assembly, even though changes in secondary structure are small.

Main Chain Conformation. Raman bands of the portal monomer and dodecamer that are diagnostic of secondary structure are enlarged for comparison in Figure 4. The amide III and amide I markers are shown in the top (1175−1375 cm^{-1} interval) and bottom panels (1500−1750 cm^{-1} interval), respectively. To reflect the actual magnitude of assembly-induced changes in Raman amide bands, the difference traces in both panels of Figure 4 are shown without ordinate expansion.

In the case of amide I (Figure 4, bottom panel), we observe small increases (∼2%) in the intensities of the α-helix marker at 1656 cm^{-1} and *β*-strand marker at 1669 cm^{-1}. Concomitant decreases occur near 1648 and 1678 cm^{-1}, where irregular conformations contribute. The difference spectrum is consistent with curve fitting results (*32*), which suggest only a marginal change in portal subunit secondary structure with assembly. It is interesting that this small change is similar to that observed with P22 procapsid maturation (*35*).

In the amide III region (Figure 4, top panel), the spectral difference profile is again consistent with only a small change in secondary structure, i.e., an increased level of α-helix at the expense of unordered conformations upon portal assembly. The larger difference feature at 1278 cm^{-1} can be explained by overlapping contributions from amino acid side chains. Tyrosines, tryptophans, and other residues contribute Raman intensity at this position (*36*).

Tyrosines. The portal subunit contains 26 tyrosines (*7*). Most (20) occur within the central 50% of the sequence (residues 223−571), and none occurs in the C-terminal segment (residues 572−725). The bottom trace of Figure 2 shows that the tyrosine marker at 852 cm^{-1} undergoes the largest assembly-related intensity change in the Raman

spectrum. This implicates the central region of the sequence in the intersubunit interface. The 852 cm^{-1} band is one member of a structurally informative Fermi interaction doublet (852/828 cm^{-1}). The Raman intensity ratio of the doublet (I_{852}/I_{828}) is diagnostic of the average phenoxyl hydrogen-bonding state of the subunit tyrosines (*37*, *38*). The data in Figure 2 show that the diagnostic ratio increases from 1.0 in the monomer to 1.3 in the ring, which indicates a large net *decrease* in the strength of hydrogen bond donation by subunit phenoxyl (O−H) sites upon portal ring assembly. Assembly-related changes in tyrosyl local environments may also contribute to the difference features observed at 1259 (trough) and 1278 cm^{-1} (peak) in Figure 2.

Tryptophans. The portal subunit contains 11 tryptophans (*7*), all but one of which are confined to the N-terminal half of the sequence. The great majority (eight) occur close to the N-terminus, between positions 19 and 211. Like the Raman markers of the subunit tyrosines (above), certain tryptophan Raman markers are perturbed significantly by portal assembly. The bottom trace of Figure 2 exhibits difference features in the following Trp Raman bands (corresponding normal modes of the indolyl ring are given in parentheses; see also Table 1): 759 (W18), 1425 (W6), and 1550 cm^{-1} (W3). The observed difference peak near 1340 cm^{-1} may also contain a contribution from Trp indoles (mode W7). Some of these spectral changes are also evident in Figure 3.

The structural significance of assembly-related changes in Trp Raman markers can be understood in terms of previously established correlations as follows. The band near 1550−1555 cm^{-1} (W3) is sensitive in position to the absolute magnitude of the indolyl side chain torsion $\chi^{2,1}$ (*39*). The observed 1554 → 1551 cm^{-1} shift indicates a change in the average indolyl $|\chi^{2,1}|$ torsion from ∼95° to ∼103° with assembly. Conversely, the Trp marker near 878 cm^{-1} (W17), which is diagnostic of relatively strong hydrogen bonding of indolyl N1−H sites (*39*), does not change appreciably with portal assembly. Although tryptophan residues may contribute to the Raman intensity increase at 1340 cm^{-1} (W7) (*40*), substantial contributions are also expected in this region from the nonaromatic side chains and the α-helical secondary structure of the subunit (Table 1). Accordingly, a simple interpretation of the structural significance of the Raman difference peak at 1334 cm^{-1} is not feasible.

Collectively, the perturbed Trp Raman markers show that significant conformational adjustments occur in the N-terminal segment of the portal subunit as a consequence of ring assembly. Thus, it appears that both the N-terminal third and middle third of the sequence are implicated in the intersubunit interface.

Cysteines. The hydrogen bonding sensitivity of the Raman sulfhydryl stretching band (2520−2600 cm^{-1} interval) is well-documented (*41*). Indeed, the Raman spectrum is unique in its ability to provide insights into the local environments of cysteine S−H sites in large assemblies (*18*, *19*). Despite the low intensities of Raman S−H signals, the four cysteines of the portal subunit (Cys 153, Cys 173, Cys 283, and Cys 516) (*7*) generate distinctive Raman S−H signatures for monomeric and dodecameric states, as shown in Figure 3.

In the case of the monomer, the Raman S−H profile is relatively broad with a central peak at 2562 cm^{-1} and a prominent shoulder of nearly equal intensity at 2557 cm^{-1}. The positions, intensities, and breadths of these overlapping bands suggest that all four cysteines in the monomer engage in relatively strong S−H···X hydrogen bonds such that two of the sulfhydryls are slightly more strongly hydrogen bonded (2557 cm^{-1} marker) than the others (2562 cm^{-1} marker). Conversely, for the dodecamer, virtually all of the Raman S−H band intensity appears to be shifted to higher wavenumber values. Thus, the dodecamer exhibits its major peak at 2566 cm^{-1}, indicative of moderately strong S−H···X hydrogen bonds, and a less intense though broader peak at 2587 cm^{-1}, corresponding to weak S−H···X hydrogen bonds. These data for the dodecamer do not identify unambiguously the population distribution between the two types of hydrogen-bonding states. However, estimation of the integrated Raman intensity ratio of the 2566 and 2587 cm^{-1} band components by curve fitting (data not shown) implies that two Cys residues populate each hydrogen-bonding state. It is noteworthy that the marker at 2587 cm^{-1} in the dodecamer is similar to that observed for a solvent-exposed sulfhydryl group (*41*). This suggests that portal assembly may disrupt two relatively strong intrasubunit ("buried") S−H···X hydrogen bonds and result in solvent exposure of the Cys sites to enable weaker S−H···OH_2 hydrogen bonds.

The difference spectrum (Figure 3, bottom trace) confirms that more than one Cys residue undergoes a dramatic change in hydrogen bonding with portal assembly and that this change is in the direction of much weaker S−H···X hydrogen bonds. Interestingly, the four cysteines of the portal subunit (Cys 153, Cys 173, Cys 283, and Cys 516), like the tyrosines and tryptophans noted above, are under-represented in the C-terminal third of the portal sequence (*7*). Again, the data are consistent with side chains of the N-terminal third and central third of the sequence undergoing large changes with portal assembly.

Oxidation of reduced cysteines to form cystine bridges in proteins is accompanied by the appearance of diagnostic S−S stretching bands in the 500−550 cm^{-1} interval of the Raman spectrum (*42*). The absence of assembly-related changes in the 500−550 cm^{-1} interval of the Raman spectrum confirms that no disulfide bridges are formed with portal assembly.

Other Side Chains. Many additional side chains are highly represented in the portal subunit sequence, including Asp (61 per subunit) and Glu (54) (*7*). Both are expected to contribute a prominent marker near 1400 cm^{-1}, which can be assigned to the symmetric stretching vibration of the ionized carboxylate (CO_2^-) group (*36*). The Raman band is observed prominently and without change in both monomer and dodecamer spectra (Figure 2), indicating that there is no net change in the ionization states of Asp and Glu residues at the experimental conditions employed. This is not unexpected for the pH 7.5 solutions examined here.

The portal subunit is also rich in basic side chains (42 Arg and 37 Lys residues) (*7*). Although most Raman markers of these side chains are relatively weak (*36*), their cumulative effect could be significant. The difference spectrum of Figure 2 reveals one feature that invites speculation regarding the possible involvement of basic side chains in portal assembly. This is the positive difference peak near 1080 cm^{-1}, which coincides with a recently proposed Raman marker of the guanido group of arginine (*43*). Unfortunately, other amino

acid side chains may contribute Raman intensity near 1080 cm^{-1} (*36*), and weak contributions may also arise from uncompensated Tris buffer. Nevertheless, we cannot exclude the possibility that a small increase in the net ionization state of subunit Arg residues accompanies portal assembly.

DISCUSSION AND CONCLUSIONS

The double-stranded DNA translocating vertex of bacteriophage P22 consists of 12 copies of an 84 kDa portal subunit. A recombinantly expressed His_6-tagged portal subunit has been purified for examination in monomeric and dodecameric states by laser Raman spectroscopy. *The Raman spectra show that portal assembly leads to only a small perturbation of subunit secondary structure but large changes in the local environments of subunit side chains*. In particular, portal assembly results in a major reorganization of cysteine S−H hydrogen-bonding states, substantial alteration of tyrosine O−H hydrogen-bonding states, and large changes in tryptophan amphipathic environments. The Raman-monitored changes in side chains indicate that the N-terminal third and central third of the portal sequence are involved in intersubunit recognition, but do not preclude involvement of the C-terminal region. The Raman results are in accord with fluorescence and CD measurements (*14*, *24*).

A preliminary examination of the Raman spectrum of the portal dodecamer in D_2O solution indicates that large deuteration shifts occur in bands associated with both the peptide main chain (amide I and amide III markers) and labile side chains (Tyr, Trp, and Cys) (A. Rodriguez-Casado, R. Tuma, S. Moore, P. E. Prevelige, Jr., and G. J. Thomas, Jr., unpublished results). Although corresponding hydrogen−deuterium exchange data have not yet been obtained for the portal monomer, the deuteration effects observed for the dodecamer are larger and more extensive than those reported for coat protein subunits of P22 procapsid and capsid shells (*17*, *18*). These results imply that subunits of the portal assembly have a less compact fold than subunits of the capsid and procapsid shell assemblies.

Recently, Tuma and co-workers employed Raman spectroscopy, small-angle X-ray scattering, and hydrogen−deuterium exchange methods to characterize subunit structural changes accompanying in vitro construction of the P22 procapsid shell from recombinantly expressed coat protein monomers (*18*). Procapsid formation results in a substantial change in the conformation of the subunit main chain, but relatively small changes in the environments of subunit side chains, including those of cysteine, tyrosine, and tryptophan. The Raman signature for procapsid shell formation thus stands in striking contrast to that of portal ring formation. This distinction may be related to the respective roles of the two subassemblies in the overall virion maturation pathway. Whereas the dodecameric ring appears to represent the *final* quaternary state of the portal subunit, the procapsid shell represents a *metastable* quaternary state that is subsequently transformed (during DNA packaging in vivo) into the mature capsid shell. Procapsid-to-capsid maturation is expected to require appreciable plasticity at intersubunit interfaces of the initially formed, metastable procapsid lattice. Conversely, the portal dodecamer undergoes no apparent structural transformation comparable to that of procapsid shell maturation. The portal dodecamer examined here is presumably competent for in vivo recognition of both the coat protein during procapsid shell formation (*14*) and viral DNA during genome packaging.

On the other hand, unlike procapsid assembly, the procapsid-to-capsid shell maturation event leads to changes in the coat protein Raman spectrum that are qualitatively and quantitatively very similar to those accompanying portal assembly, namely, large-scale changes in side chain environments but a relatively small change in the main chain conformation (*17*, *35*). Thus, the Raman difference signature diagnostic of portal formation (bottom traces of Figures 2−4), though distinct from that of procapsid formation (*17*), is comparable to the Raman difference signature diagnostic of capsid maturation (*35*). In terms of the subunit structural response monitored by Raman spectroscopy, the dodecamerization of the portal monomer more closely resembles the procapsid-to-capsid transfomation than the construction of the procapsid from coat protein monomers. Extensive changes in side chain environments without an appreciable change in secondary structure may be common to supramolecular organization processes not requiring structural intermediates and not dependent upon plasticity at subunit interfaces. The distinctive portal and coat protein assembly pathways and their respective Raman characteristics are represented schematically in Figure 5.

Conservation of quaternary structure among portal assemblies from diverse DNA bacteriophages has been noted previously (*6*). This suggests that secondary and tertiary structure modules may also be conserved among the respective portal subunits. The recent determination of the X-ray crystal structure of the bacteriophage φ29 portal assembly by Rossmann, Anderson, and co-workers (*9*) provides a convenient opportunity to evaluate whether secondary structure modules might be conserved between subunits of the φ29 and P22 portals. Accordingly, we analyzed the corresponding sequences using the program META PredictProtein (http://www.embl-heidelberg.de/predictprotein/doc/meta_intro.html). Although the φ29 and P22 portal subunits exhibit no significant sequence homology, an extended segment of the P22 subunit (viz. residues 240−350) is predicted to have a series of secondary structure modules that map closely with corresponding modules of the φ29 subunit, as shown in Figure 6A. It is interesting that the predicted structure homology involves the inner annular surface of the φ29 portal, i.e., the channel through which DNA passage is presumed to occur during packaging and ejection events. The relevant domain of the φ29 portal subunit is shown in the three-dimensional structure of Figure 6B. No other extensive secondary structure homologies are evident between the φ29 and P22 subunits. The alignment scheme of Figure 6A suggests that residues 240−350 of the P22 subunit may represent a conserved evolutionary domain of importance in DNA translocating functions of the virion. It is also noteworthy that 27% (21 of 79) of the basic side chains of the P22 subunit are localized within 15% of the sequence (residues 240−350). Such a high density of basic side chains might mediate genome translocation by facilitating transient binding to DNA phosphates. In further support of this hypothesis, we note that residues 240−350 of the P22 portal subunit are resistant to the chymotrypsin digestion that cleaves other segments of the protein (*14*).

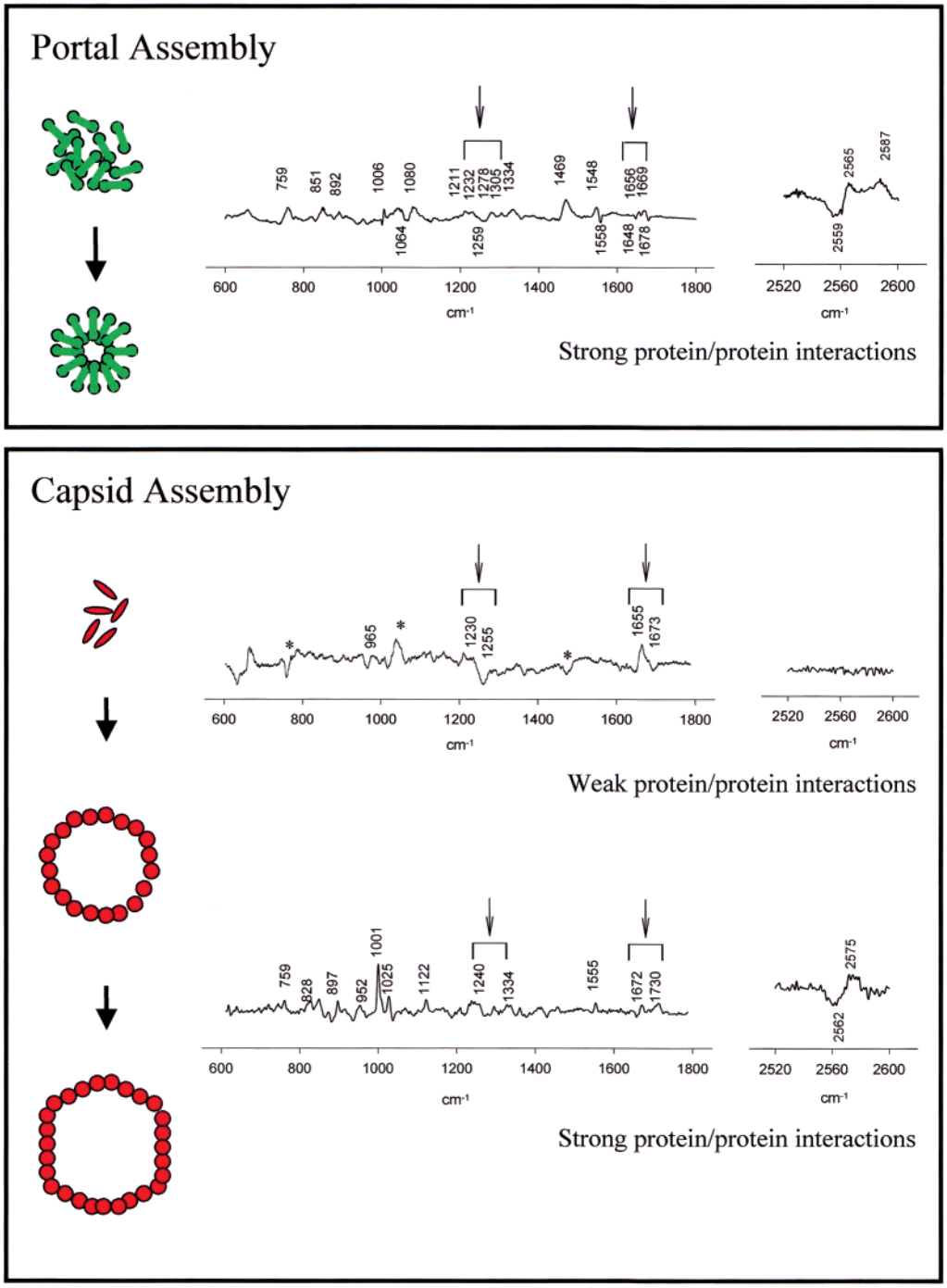

FIGURE 5: Schematic representation of in vitro assembly pathways and corresponding Raman signatures for P22 portal (top panel) and coat (bottom panel) subunits. For the portal, the mature dodecameric quaternary state forms directly from monomers. The Raman difference signature is distinguished by relatively large changes in the marker bands of cysteine (right trace, 2520−2600 cm^{-1}) and other side chains (left trace, 600−1800 cm^{-1}), but relatively small changes in amide I and III markers of the main chain conformation (arrows). For the coat, a metastable procapsid shell as well as the monomer and mature capsid can be characterized. For the first stage of capsid assembly, the Raman difference signature is distinguished by little or no changes in side chain Raman markers of cysteine (right trace) and other side chains (left trace), but relatively large changes in amide I and III markers (arrows). (Note that difference features labeled with asterisks are due to uncompensated buffer.) This contrasts sharply with the portal (cf. top panel). For the second stage of capsid assembly, the Raman difference signature is distinguished by relatively large changes in side chain Raman markers of cysteine (right trace) and other side chains (left trace), but relatively small changes in amide I and III markers (arrows). This is analogous to the portal (cf. top panel). The distinct Raman difference profiles of portal and coat assemblies are proposed to be representative of the two types of pathways (see the text).

The 725-residue subunit of the P22 portal must also contain structural modules not present in the fold of the 309-residue φ29 subunit. On the basis of Figure 6A, the additional modules are most likely C-terminal to the putative conserved region. Such domains might be utilized in recognition of capsid and tailspike proteins, as well as in fulfilling functions of the pRNA cofactor that is present in φ29 but absent from P22. It is also possible that the additional structural modules of the P22 subunit might have evolved to provide specific functions associated with P22 DNA packaging. In fact, two mutations in the P22 portal protein have been associated with determining the density of viral genome packaging (*44*). One

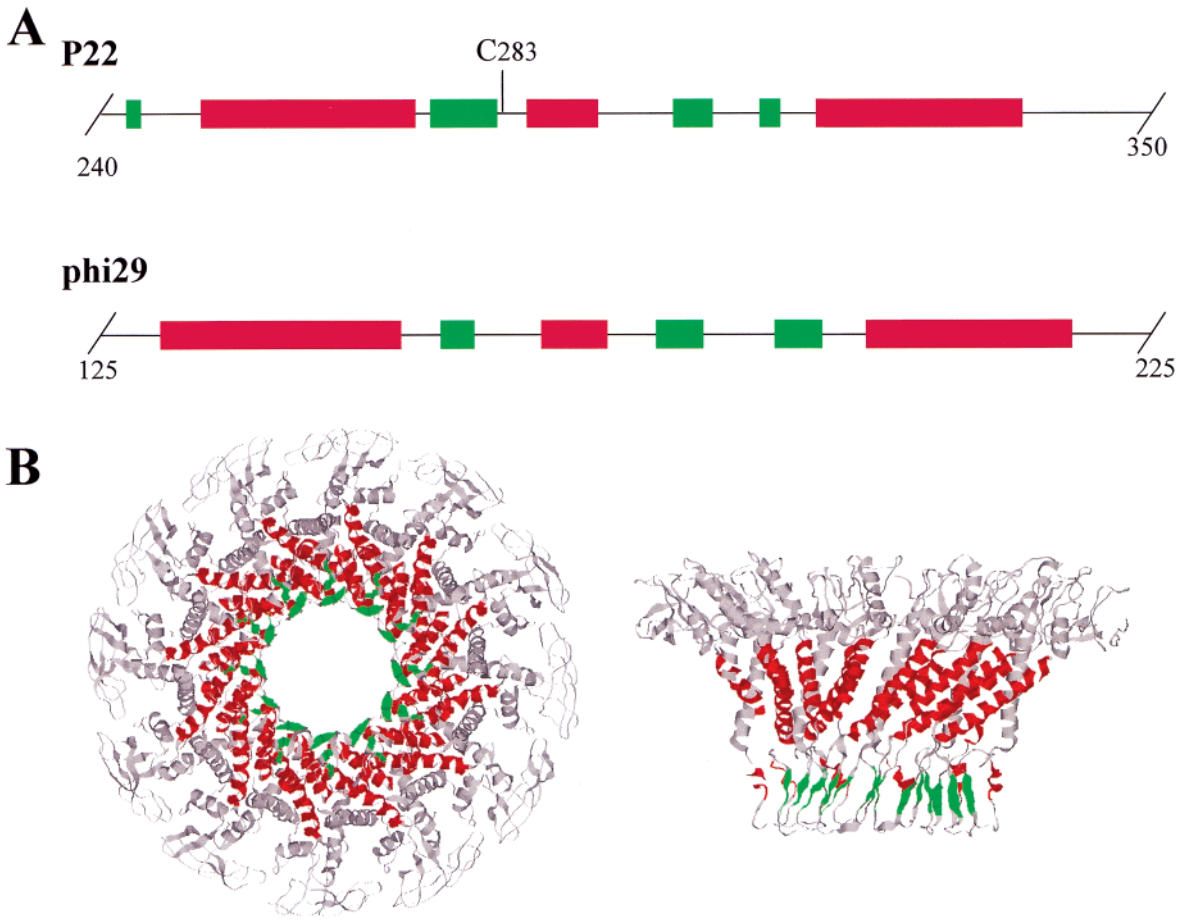

FIGURE 6: (A) Conserved secondary structure modules in the portal proteins of bacteriophages P22 (residues 240−350) and φ29 (residues 125−225). Both sequences were analyzed for secondary structure content using the program META PredictProtein (www.embl-heidelberg.de/predictprotein/doc/meta_intro.html) to generate the results that are shown. In the case of φ29, the prediction agrees well with the X-ray crystal structure of Simpson et al. (Protein Data Bank entry 1FOU) (*9*). In the case of P22, the prediction yields 46% α-helix and 12% β-sheet, in good agreement with Raman and CD data. Regions of α-helix (red) and β-strand (green) are drawn to scale, and boundary residues are numbered. (B) The three-dimensional structure of the φ29 portal dodecamer (PDB entry 1FOU). Regions of α-helix (red) and β-strand (green) are color coded as in panel A. Regions rendered in gray fall outside the putative conserved domain.

of these, Val 64 → Met, is actually N-terminal to the putative conserved domain, whereas the other, Met 303 → Val, is within it. Cross-talk between the conserved DNA sensing region of the P22 protein (residues 240−350) and the external packaging machinery (terminase and host factors) may also be mediated by structural modules present in the P22 protein but absent from the φ29 protein. Simpson et al. (*9*) have proposed that translocations of α-helices comprising the walls of the φ29 annulus may mediate packaging of the φ29 genome.

Finally, the surprisingly large sensitivity of the Raman sulfhydryl signature of the portal subunit to the state of assembly (Figure 3) may be of biological significance. We note that a recent investigation of single-site Cys → Ser mutants of the trimeric tailspike of phage P22 has demonstrated five different Raman sulfhydryl markers comprising seven distinct sulfhydryl hydrogen-bonding states for the eight cysteines per tailspike subunit (*19*). A subset of these eight cysteines is crucial to the folding and assembly pathway of the native tailspike trimer. The cysteine signature of the P22 portal protein, although less complex than that of the tailspike protein, is nevertheless also demonstrably sensitive to the assembly pathway. At least one portal cysteine (Cys 283) falls within the putative conserved domain that may function in DNA translocation. In future work, single-site Cys → Ser mutants of the portal protein will be constructed to identify the distinct Raman S−H markers and hydrogen-bonding states specific to each cysteine sulfhydryl.

ACKNOWLEDGMENT

We thank Dr. James M. Benevides for comments on the manuscript.

NOTE ADDED IN PROOF

The symmetry mismatch between the portal and head assemblies of bacteriophage φ29 have been further discussed in two recently published papers (*48*, *49*).

REFERENCES

1. King, J., Lenk, E. V., and Botstein, D. (1973) *J. Mol. Biol. 80*, 697−731.
2. Casjens, S., and Hendrix, R. (1988) in *The Bacteriophages* (Calendar, R., Ed.) pp 15−91, Plenum, New York.
3. Rixon, F. J. (1993) *Semin. Virol. 4*, 135−144.
4. Prevelige, P. E., Jr., and King, J. (1993) *Prog. Med. Virol. 40*, 206−221.
5. King, J., and Chiu, W. (1997) in *Structural Biology of Viruses* (Chiu, W., Burnett, R. M., and Garcea, R., Eds.) pp 288−311, Oxford University Press, New York.

6. Bazinet, C., and King, J. (1985) *Annu. Rev. Microbiol. 39*, 109−129.
7. Eppler, K., Wyckoff, E., Goates, J., Parr, R., and Casjens, S. (1991) *Virology 183*, 519−538.
8. Valpuesta, J. M., and Carrascosa, J. L. (1994) *Q. Rev. Biophys. 27*, 107−155.
9. Simpson, A. A., Tao, Y., Leiman, P. G., Badasso, M. O., He, Y., Jardine, P. J., Olson, N. H., Morais, M. C., Grimes, S., Anderson, D. L., Baker, T. S., and Rossmann, M. G. (2000) *Nature 408*, 745−750.
10. Valpuesta, J. M., Fernandez, J. J., Carazo, J. M., and Carrascosa, J. L. (1999) *Structure 7*, 289−296.
11. Valle, M., Kremer, L., Martinez, A., Roncal, F., Valpuesta, J. M., Albar, J. P., and Carrascosa, J. L. (1999) *J. Mol. Biol. 288*, 899−909.
12. Orlova, E. V., Dube, P., Beckmann, E., Zemlin, F., Lurz, R., Trautner, T. A., Tavares, P., and van Heel, M. (1999) *Nat. Struct. Biol. 6*, 842−846.
13. Dröge, A., and Tavares, P. (2000) *J. Mol. Biol. 296*, 103−115.
14. Moore, S. D., and Prevelige, P. E., Jr. (2001) *J. Biol. Chem. 276*, 6779−6788.
15. Hendrix, R. W. (1978) *Proc. Natl. Acad. Sci. U.S.A. 75*, 4779−4783.
16. Tuma, R., and Thomas, G. J., Jr. (1997) *Biophys. Chem. 68*, 17−31.
17. Tuma, R., Prevelige, P. E., Jr., and Thomas, G. J., Jr. (1998) *Proc. Natl. Acad. Sci. U.S.A. 95*, 9885−9890.
18. Tuma, R., Tsuruta, H., Benevides, J. M., Prevelige, P. E., Jr., and Thomas, G. J., Jr. (2001) *Biochemistry 40*, 665−674.
19. Raso, S. W., Clark, P. L., Haase-Pettingell, C., King, J. A., and Thomas, G. J., Jr. (2001) *J. Mol. Biol. 307*, 899−911.
20. Tuma, R., Bamford, J. K. H., Bamford, D. H., Russell, M. P., and Thomas, G. J., Jr. (1996) *J. Mol. Biol. 257*, 87−101.
21. Tuma, R., Bamford, J. K. H., Bamford, D. H., and Thomas, G. J., Jr. (1999) *Biochemistry 38*, 15025−15033.
22. Benevides, J. M., Juuti, J. T., Tuma, R., Bamford, D. H., and Thomas, G. J., Jr. (2001) *J. Virol.* (submitted for publication).
23. Gill, S. C., and von Hippel, P. H. (1989) *Anal. Biochem. 182*, 319−326.
24. Sreerama, N., and Woody, R. W. (1994) *J. Mol. Biol. 242*, 497−507.
25. Movileanu, L., Benevides, J. M., and Thomas, G. J., Jr. (1999) *J. Raman Spectrosc. 30*, 637−649.
26. Carey, P. R. (1999) *J. Biol. Chem. 274*, 26625−26628.
27. Dong, J., Dinakarpandian, D., and Carey, P. R. (1998) *Appl. Spectrosc. 52*, 1117−1122.
28. Thomas, G. J., Jr. (1999) *Annu. Rev. Biophys. Biomol. Struct. 28*, 1−27.
29. Overman, S. A., and Thomas, G. J., Jr. (1998) *J. Raman Spectrosc. 29*, 23−29.
30. Tsuboi, M., Suzuki, M., Overman, S. A., and Thomas, G. J., Jr. (2000) *Biochemistry 39*, 2677−2684.
31. Tuma, R., and Thomas, G. J., Jr. (2001) in *Handbook of Vibrational Spectroscopy, Volume 5, Applications of Vibrational Spectroscopy in Biochemistry, Biomedicine and Pharmaceutical Science* (Chalmers, J. M., and Griffiths, P. R., Eds.) John Wiley & Sons, Chichester, U.K. (in press).
32. Berjot, M., Marx, J., and Alix, A. J. P. (1987) *J. Raman Spectrosc. 18*, 289−300.
33. Bandekar, J. (1992) *Biochim. Biophys. Acta 1120*, 123−143.
34. Tuma, R., Prevelige, P. E., and Thomas, G. J., Jr. (1996) *Biochemistry 35*, 4619−4627.
35. Prevelige, P. E., Jr., Thomas, D., King, J., Towse, S. A., and Thomas, G. J., Jr. (1993) *Biochemistry 32*, 537−543.
36. Overman, S. A., and Thomas, G. J., Jr. (1999) *Biochemistry 38*, 4018−4027.
37. Siamwiza, M. N., Lord, R. C., Chen, M. C., Takamatsu, T., Harada, I., Matsuura, H., and Shimanouchi, T. (1975) *Biochemistry 14*, 4870−4876.
38. Arp, Z., Autrey, D., Laane, J., Overman, S. A., and Thomas, G. J., Jr. (2001) *Biochemistry 40*, 2522−2529.
39. Miura, T., Takeuchi, H., and Harada, I. (1989) *J. Raman Spectrosc. 20*, 667−671.
40. Harada, I., Miura, T., and Takeuchi, H. (1986) *Spectrochim. Acta 42A*, 307−312.
41. Li, H., and Thomas, G. J., Jr. (1991) *J. Am. Chem. Soc. 113*, 456−462.
42. Lord, R. C., and Yu, N.-T. (1970) *J. Mol. Biol. 50*, 509−524.
43. Tsuboi, M., Aida, M., Nakamura, K., Bondre, P., Overman, S. A., Benevides, J. M., and Thomas, G. J., Jr. (2001) *Biophys. J. 80*, 397a.
44. Casjens, S., Wyckoff, E., Hayden, M., Sampson, L., Eppler, K., Randall, S., Moreno, E. T., and Serwer, P. (1992) *J. Mol. Biol. 224*, 1055−1074.
45. Miura, T., and Thomas, G. J., Jr. (1995) in *Proteins: Structure, Function and Engineering* (Biswas, B. B., and Roy, S., Eds.) pp 55−99, Plenum, New York.
46. King, J., Botstein, D., Casjens, S., Earnshaw, W., Harrison, S., and Lenk, E. (1976) *Philos. Trans. R. Soc. London, Ser. B 276*, 37−49.
47. Casjens, S., and King, J. (1975) *Annu. Rev. Biochem. 44*, 555−611.
48. Simpson, A. A., Leiman, P. G., Tao, Y., He, Y., Badasso, M. O., Jardine, P. J., Anderson, D. L., and Rossmann, M. G. (2001) Structure determination of the head-tail connector of bacteriophage φ29. *Acta Crystallogr. D. Biol. Crystallogr. 57*, 1260−1269.
49. Morais, M. C., Tao, Y., Olson, N. H., Grimes, S., Jardine, P. J., Anderson, D. L., Baker, T. S., and Rossmann, M. G. (2001) Cryoelectron-microscopy image reconstruction of symmetry mismatches in bacteriophage φ29. *J. Struct. Biol. 135*, 38−46.

BI0110488